
HYBRID QUANTUM-CLASSICAL BRANCH-AND-PRICE FOR INTRA-DAY ELECTRIC VEHICLE CHARGING SCHEDULING VIA PARTITION COLORING

Peng Sun

College of Management and Economics
Tianjin University
Tianjin, 300072, China
sunpeng1317@tju.edu.cn

Liang Zhong

College of Management and Economics
Tianjin University
Tianjin, 300072, China
zl-2002@tju.edu.cn

Qing-Guo Zeng

Shenzhen Institute for Quantum Science and Engineering
Southern University of Science and Technology
Shenzhen, 518055, China
zengqg2022@mail.sustech.edu.cn

Li Wang*

College of Economics and Management
Hebei University of Technology
Tianjin, 300130, China
li.wang@hebut.edu.cn

March 24, 2026

ABSTRACT

The rapid deployment of electric vehicles (EVs) in public parking facilities and fleet operations raises challenging intra-day charging scheduling problems under tight charger capacity and limited dwell times. We model this problem as a variant of the Partition Coloring Problem (PCP), where each vehicle defines a partition, its candidate charging intervals are vertices, and temporal and resource conflicts are represented as edges in a conflict graph. On this basis, we design a branch-and-price algorithm in which the restricted master problem selects feasible combinations of intervals, and the pricing subproblem is a maximum independent set problem. The latter is reformulated as a quadratic unconstrained binary optimization (QUBO) model and solved by quantum-annealing-inspired algorithms (QAIA) implemented in the MindQuantum framework, specifically the ballistic simulated branching (BSB) and simulated coherent Ising machine (SimCIM) methods, while the master problem is solved by Gurobi. Computational experiments on a family of synthetic EV charging instances show that the QAIA-enhanced algorithms match the pure Gurobi-based branch-and-price baseline on small and medium instances, and clearly outperform it on large and hard instances. In several cases where the baseline reaches the time limit with non-zero optimality gaps, the QAIA-based variants close the gap and prove optimality within the same time budget. These results indicate that integrating QAIA into classical decomposition schemes is a promising direction for large-scale EV charging scheduling and related PCP applications.

1 Introduction

In recent years, the widespread adoption of electric vehicles (EVs) in public parking facilities, workplace charging stations, and large fleet operations has made intra-day charging scheduling an important operational optimization problem. Unlike conventional refueling, EV charging is time-consuming and highly flexible; it is influenced by users' departure deadlines, power-capacity limitations, and fluctuations in instantaneous charging load. In typical intra-day scenarios, vehicles arrive and depart within the same day and expect to obtain sufficient energy during a limited dwell period to support subsequent trips. Consequently, operators must assign feasible charging intervals to each vehicle under restricted resources while balancing demand satisfaction, charger utilization, and overall system stability.

*Corresponding Author

The literature has examined the EV charging scheduling problem from multiple perspectives. For instance, Dolgui et al. [1] formulated a scheduling model for conventional charging tasks with parallel chargers and explicitly characterized task–resource conflicts, while Wang et al. [2] developed an integrated framework that jointly models daily mobility patterns and charging activities. In addition, Shen et al. [3] proposed a two-stage method that coordinates vehicle–charger matching and bidirectional charging strategies under photovoltaic uncertainty. Data-driven and heuristic approaches, including deep learning [4], reinforcement learning [5, 6], and genetic algorithms [7], have also been widely applied to derive near-optimal charging policies in complex environments.

Most existing studies rely on time-indexed integer programming models. By discretizing vehicles’ dwell windows, scheduling decisions are mapped to binary assignments between vehicles and time slots. Although effective for small and medium instances, this modeling approach has inherent limitations. The model size grows rapidly as the temporal resolution increases; conflict relationships among candidate charging intervals, such as temporal overlap, sharing of physical chargers, or local load interactions, are only implicitly represented; and the number of constraints and variables escalates quickly with the number of vehicles and candidate intervals. As a result, conventional MILP formulations face substantial challenges in large-scale, continuous-time, or multi-resource coupled settings.

Graph-based formulations offer a natural way to represent conflicts, particularly for capturing the mutual exclusivity of candidate charging intervals. Recent work has shown that the scheduling problem can be reformulated as a vertex coloring problem and solved using the Quantum Approximate Optimization Algorithm (QAOA) [8]. However, EV scheduling exhibits a specific structural characteristic: each vehicle may have several candidate intervals, but only one can be selected. This “vehicle as partition, interval as vertex, exactly one vertex selected per partition” structure corresponds more closely to the Partition Coloring Problem (PCP). Although the PCP has been studied in combinatorial optimization [9, 10, 11], it has not been systematically applied to EV charging scheduling.

To address this gap, we model the intra-day EV charging scheduling problem as a variant of PCP. Each vehicle is treated as a partition, and its candidate charging intervals constitute the vertices within that partition. For example, if a vehicle has three candidate intervals A1, A2, and A3, they form one partition in the graph. Edges connect vertices whose intervals overlap or share conflicting physical or electrical resources. Given a limited number of chargers C , the goal is to select a maximum independent set that minimizes the latest completion time while selecting exactly one interval per vehicle and satisfying resource constraints.

Based on this modeling framework, our main contributions are as follows:

1. We provide the first systematic formulation of the intra-day EV charging scheduling problem as a PCP, enabling explicit representation of vehicle-level and interval-level conflicts while naturally supporting multiple resource constraints.
2. We develop a Branch-and-Price algorithm in which the master problem handles partition selection and resource allocation, and the pricing subproblem generates new columns via a maximum independent set structure, thereby improving computational efficiency.
3. We integrate a quantum annealing-inspired algorithm (QAIA) solver implemented in the MindSpore Quantum framework to accelerate the pricing subproblem and enhance scalability for large problem instances.

Finally, we conduct extensive numerical experiments comparing the proposed QAIA-enhanced branch-and-price algorithms with a pure Gurobi-based baseline on synthetic EV charging instances of varying sizes, demonstrating that the QAIA-based methods significantly improve performance on large and hard cases while preserving optimal solution quality.

The remainder of this paper is organized as follows. Section 2 reviews the literature on EV charging scheduling and related optimization approaches. Section 3 describes the problem. Section 4 presents the formal mathematical formulation. Section 5 reports the computational experiments and compares a pure Gurobi-based branch-and-price baseline with two QAIA-based pricing variants (BSB and SimCIM) on a family of PCP instances derived from EV charging scenarios. Finally, Section 6 concludes the paper and outlines potential directions for future research.

2 Related Works

2.1 Electric Vehicle Charging Scheduling

EVs have been increasingly adopted in logistics and urban delivery systems. Their limited driving range and charging requirements make joint fleet scheduling and charging optimization a critical research topic in transportation and operations research. Existing studies mainly focus on routing and charging modeling, solution algorithms, and intelligent scheduling frameworks.

Routing problems with partial charging and realistic operational constraints have been extensively studied. Extensions of the electric vehicle routing problem incorporate parcel lockers, heterogeneous fleets, multiple depots, repeated customer visits, and partial recharging strategies, and are typically addressed using advanced metaheuristics such as ALNS, VNS, and VND [12, 13]. The impact of different charging models on battery degradation, travel time, and fleet size has also been analyzed, together with a systematic discussion of algorithmic applicability and modeling trade-offs [14, 15]. To cope with large-scale and dynamic environments, various intelligent and approximate solution methods have been proposed. Hybrid heuristic frameworks combine swarm intelligence with dynamic programming for personalized charging route planning [16], while survey studies summarize recent advances in two-echelon EV routing and charging coordination [17]. Dynamic decision-making under uncertainty has been addressed using Markov decision processes that incorporate charging station occupancy information [18], and deep reinforcement learning has been widely applied to jointly optimize routing, charging station selection, and dwelling time in vehicular edge computing and smart charging networks [19].

Exact and decomposition-based optimization methods have also attracted increasing attention. Column generation frameworks based on multigraph reformulation, bidirectional pricing, and graph sparsification have demonstrated strong performance on medium- to large-scale instances [20, 21], while recent reviews provide a comprehensive overview of deterministic EV charging task scheduling models and their computational properties [1]. In addition, quantum computing techniques have been explored as emerging alternatives, where EV charging scheduling problems are mapped to vertex coloring formulations and solved using QAOA or related paradigms [22, 8]. Reinforcement learning methods based on Markov decision processes and their challenges in EV scheduling have also been systematically reviewed [23].

2.2 Partition Coloring Problem

The PCP models wavelength routing and assignment in optical networks by requiring the selection of exactly one vertex from each partition, subject to the constraint that conflicting paths cannot share the same physical resource [24]. The authors proved that PCP is NP-complete, establishing its theoretical hardness and motivating subsequent algorithmic research. From a modeling perspective, PCP can be regarded as a generalization of the classical Vertex Coloring Problem (VCP). Unlike VCP, the vertex set in PCP is divided into mutually disjoint subsets, and a feasible solution requires selecting one vertex from each subset before assigning colors to the induced subgraph. This additional combinatorial structure substantially increases problem complexity and necessitates specialized solution techniques.

Recent studies have investigated both exact and heuristic approaches for solving PCP. Exact solution frameworks based on decomposition and cutting plane techniques have been shown to improve computational efficiency on small and medium sized instances [25, 26], while hybrid methods that combine set packing formulations with Branch and Price algorithms achieve high solution quality and improved scalability [27]. For large scale instances, metaheuristic approaches such as ant colony optimization demonstrate good performance and robustness [28]. Hardware accelerated solvers, including digital annealers for quadratic unconstrained binary optimization, have also been explored as alternative solution paradigms for PCP [11]. On the theoretical side, PCP has been linked to selective coloring, weighted coloring, and independent set problems, further enriching its modeling and algorithmic foundations [10]. These connections have enabled PCP to serve as a powerful abstraction for a variety of complex resource allocation problems, including electric vehicle charging scheduling and spectrum assignment [29].

2.3 Quantum Annealing Inspired Algorithm

Many combinatorial optimization problems can be formulated as Ising models, consisting of N spins $\sigma_i \in \{\pm 1\}$ with pairwise couplings J_{ij} and local fields h_i , whose energy is given by

$$H = \frac{1}{2} \sum_{i,j} J_{ij} \sigma_i \sigma_j + \sum_i h_i \sigma_i.$$

Finding the ground state of the Ising Hamiltonian is NP-hard in general [30]. To address this challenge, a class of QAIA has been developed, motivated by both dedicated hardware and their classical simulations.

At the hardware level, representative realizations include coherent Ising machines (CIM), digital annealers, and other physics-inspired computing architectures [31, 32, 33, 34]. At the algorithmic level, QAIA emulates the underlying physical dynamics on classical computers, with prominent examples including simulated CIM (SimCIM)[35] and simulated bifurcation (SB) algorithms [36]. These methods typically relax discrete spins into continuous variables and explore the energy landscape via annealing or bifurcation dynamics. Various correction mechanisms have been proposed to reduce errors induced by continuous relaxation, such as chaotic feedback and amplitude control strategies [37, 38, 39].

In this work, we adopt SimCIM and ballistic simulated bifurcation (bSB) as QAIA solvers for the pricing subproblem. SimCIM performs annealing-based optimization over continuous spin variables, while bSB enhances robustness by introducing inelastic boundary constraints to suppress analog errors during bifurcation dynamics. By leveraging the fast convergence and scalability of these QAIA methods, the proposed framework efficiently solves tightly coupled subproblems arising in large-scale combinatorial optimization.

3 Problem Description

This study considers a day-ahead charging scheduling problem for a fleet of EVs. The system configuration is illustrated in Fig. 1. The charging station is equipped with C identical chargers, and each vehicle i arrives at the station at a known time. For every vehicle, a set of feasible charging intervals is pre-generated based on its arrival time, departure deadline, and energy requirement. As shown in Fig. 1, four vehicles are depicted, each associated with three candidate intervals, and each vehicle must select exactly one interval from its corresponding set.

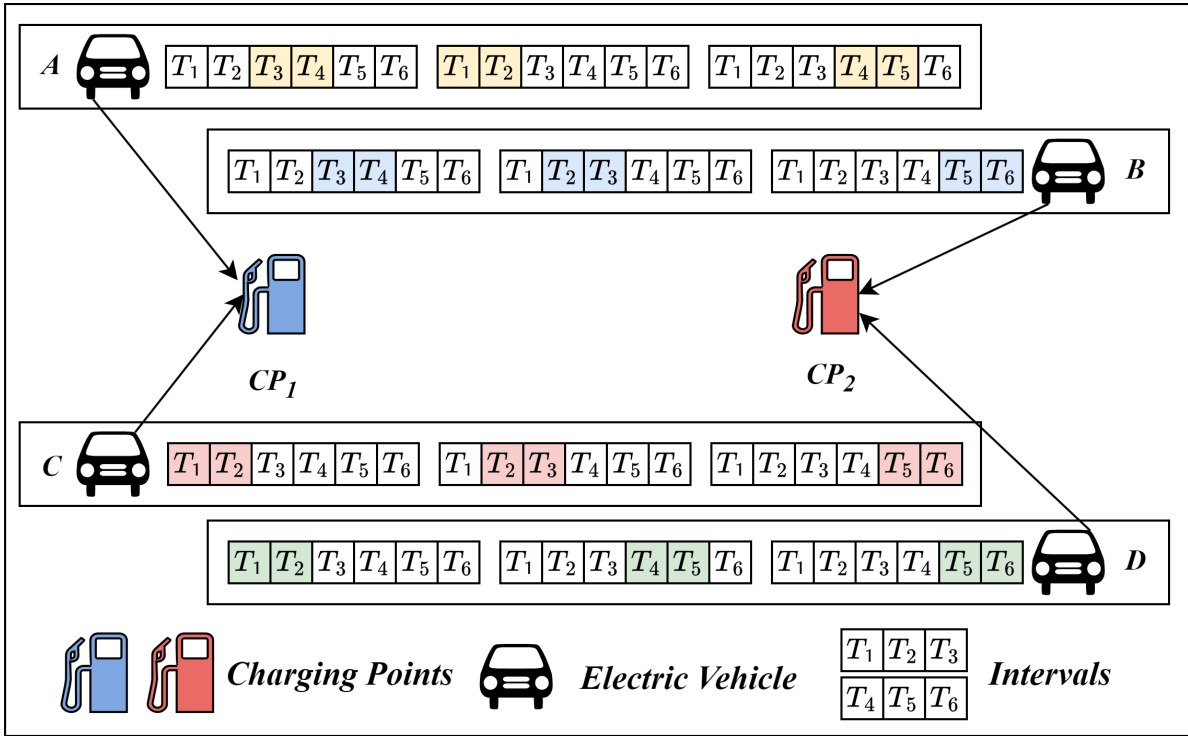


Figure 1: Schematic illustration of the EV charging system. The station contains two chargers, and four EVs are shown, each associated with three candidate intervals. The figure emphasizes the one-to-many relationship between each vehicle and its feasible intervals, without an explicit time axis.

To formalize the scheduling problem, we adopt the time-based representation shown in Fig. 2. The horizontal axis represents time, and the vertical axis lists the vehicles. Each colored bar corresponds to one candidate interval, and the intervals associated with the same vehicle form a partition. Two intervals are said to be in conflict if they overlap in time or if they belong to the same vehicle. A feasible charging schedule must therefore satisfy: (i) exactly one interval is selected for each vehicle; (ii) the number of simultaneous charging intervals at any time does not exceed the charger capacity C ; and (iii) the maximum completion time among the selected intervals, i.e., the makespan of the schedule, is minimized.

To formalize the problem, let $G = (\mathcal{V}, \mathcal{E}^A)$ be the auxiliary (conflict) graph induced by all candidate charging intervals of the electric vehicles. Each vehicle $n \in N$ is associated with a set of candidate charging intervals, each corresponding to a vertex $v \in \mathcal{V}$. The vertices associated with vehicle n form a partition $P_n \subseteq \mathcal{V}$, and the entire candidate set yields a partition of the vertex set $\mathcal{P} = \{P_n \mid n \in N\}$, with one part per vehicle. An edge $(u, v) \in \mathcal{E}^A$ exists if the corresponding intervals overlap in time or if u and v belong to the same partition P_n , i.e., they correspond to alternative intervals of the same vehicle.

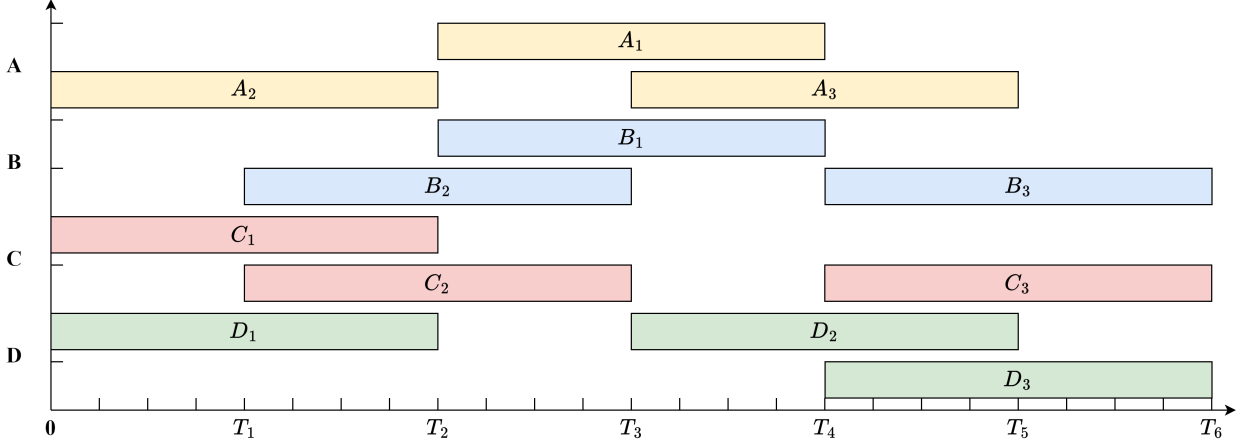


Figure 2: Illustration of candidate charging intervals with explicit temporal alignment. The horizontal axis represents time, and the vertical axis lists vehicles A , B , C , and C . Each colored bar represents a candidate interval (e.g., A_1 , A_2 , A_3). Overlapping intervals across or within vehicles indicate conflicts, which form the edge set of the conflict graph used in the PCP formulation.

An independent set is a subset $S \subseteq \mathcal{V}$ such that no two vertices in S are adjacent, i.e., $\forall u, v \in S, (u, v) \notin \mathcal{E}^A$. The charging interval selection and scheduling problem can be modeled as a Partition Coloring Problem (PCP), where the goal is to find a partial coloring $\tilde{\mathcal{C}} = \{S_1, \dots, S_h\}$ of G , with each color class S_j being a non-empty independent set, and the set of colored vertices given by $\tilde{\mathcal{V}} = \bigcup_{j=1}^h S_j$. Let $f(v)$ denote the color assigned to vertex $v \in \tilde{\mathcal{V}}$.

A feasible PCP solution must satisfy the following conditions: (i) exactly one candidate charging interval is selected for each vehicle, i.e., $|\tilde{\mathcal{V}} \cap P_n| = 1$ for all $n \in N$; (ii) no two vertices $u, v \in \mathcal{V}$ that are in conflict, i.e., $(u, v) \in \mathcal{E}^A$, are assigned the same color, ensuring that each color class represents a set of charging intervals that can be executed simultaneously without conflict; and (iii) the number of charging piles used is minimized, i.e., $\min \sum_{c \in \mathcal{C}} y_c$, where y_c is a binary variable indicating whether pile c is used.

Under this formulation, each color class corresponds to a feasible subset of non-conflicting charging intervals that can be assigned to a single charging pile. Therefore, solving the PCP is equivalent to selecting independent sets that satisfy both the partition and conflict constraints while minimizing the number of piles required. Each independent set selected in this way corresponds to a candidate column in the RMP, and the column generation procedure ensures that the resulting schedule is feasible and efficiently utilizes the available charging piles.

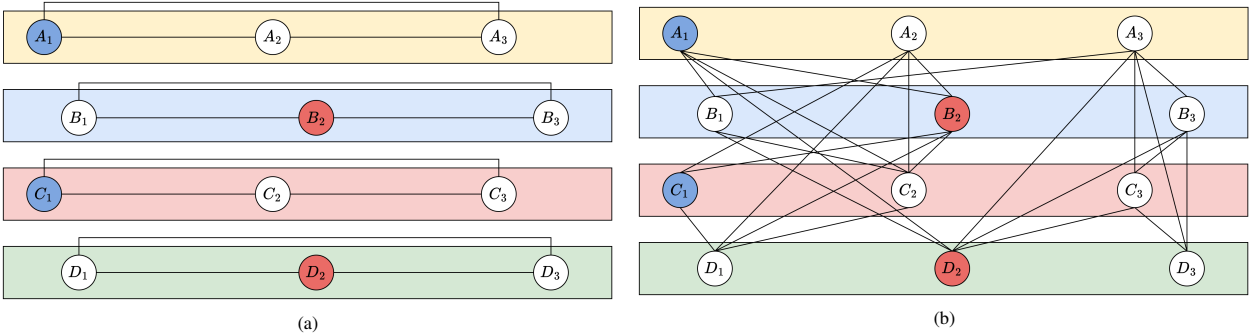


Figure 3: Construction of the conflict graph for candidate charging intervals. Subfigure (a) illustrates intra-vehicle conflicts: for each vehicle (A , B , C , and D), the three candidate intervals (e.g., A_1 , A_2 , A_3) form a clique, as only one interval can be selected for charging; therefore, all vertices associated with the same vehicle are mutually connected. Subfigure (b) illustrates inter-vehicle conflicts: vertices corresponding to different vehicles are connected if their time windows overlap, indicating that these intervals cannot be scheduled simultaneously under limited charger capacity. In addition, the vertices A_1 and C_1 are highlighted in blue to indicate that these two intervals are compatible and can share the same charger. Similarly, B_2 and D_2 are highlighted in red, illustrating another pair of mutually compatible intervals.

To provide an intuitive illustration of the problem and its graph-based formulation, Fig. 2 depicts the candidate charging intervals over time for three example vehicles, where each horizontal bar represents a potential charging interval and overlapping bars indicate conflicts. These intervals are then transformed into vertices in a conflict graph, as shown in Fig. 3, with edges representing temporal or resource conflicts between intervals. Four example feasible solutions are also presented, illustrating how independent sets in the conflict graph correspond to valid charging schedules under different charger availability scenarios. Together, these figures clearly demonstrate how the temporal scheduling problem can be reformulated as a Partition Coloring Problem for modeling purposes.

4 Methodology

To address the aforementioned problem, the overall solution workflow is illustrated in Fig. 4. The proposed algorithmic framework follows a structured four-stage process. First, all feasible charging intervals are generated for each EV, and a conflict graph is constructed based on pairwise temporal overlaps among intervals. Second, the restricted master problem (RMP) is solved within a column-generation scheme to obtain dual information that guides the search for improving columns. Third, the pricing subproblem is formulated as a QUBO model and solved using quantum annealing, while the original pricing problem is also solved via Gurobi to provide an exact benchmark for performance comparison. Finally, a customized branch-and-bound strategy, built upon interval partitioning and pairwise conflict structures, is incorporated to ensure integrality of the final solution and completeness of the overall algorithm. This workflow enables consistent treatment of interval conflicts, station capacity limitations, and the one-interval-per-vehicle requirement throughout the optimization process, thereby ensuring solution feasibility, algorithmic stability, and computational efficiency.

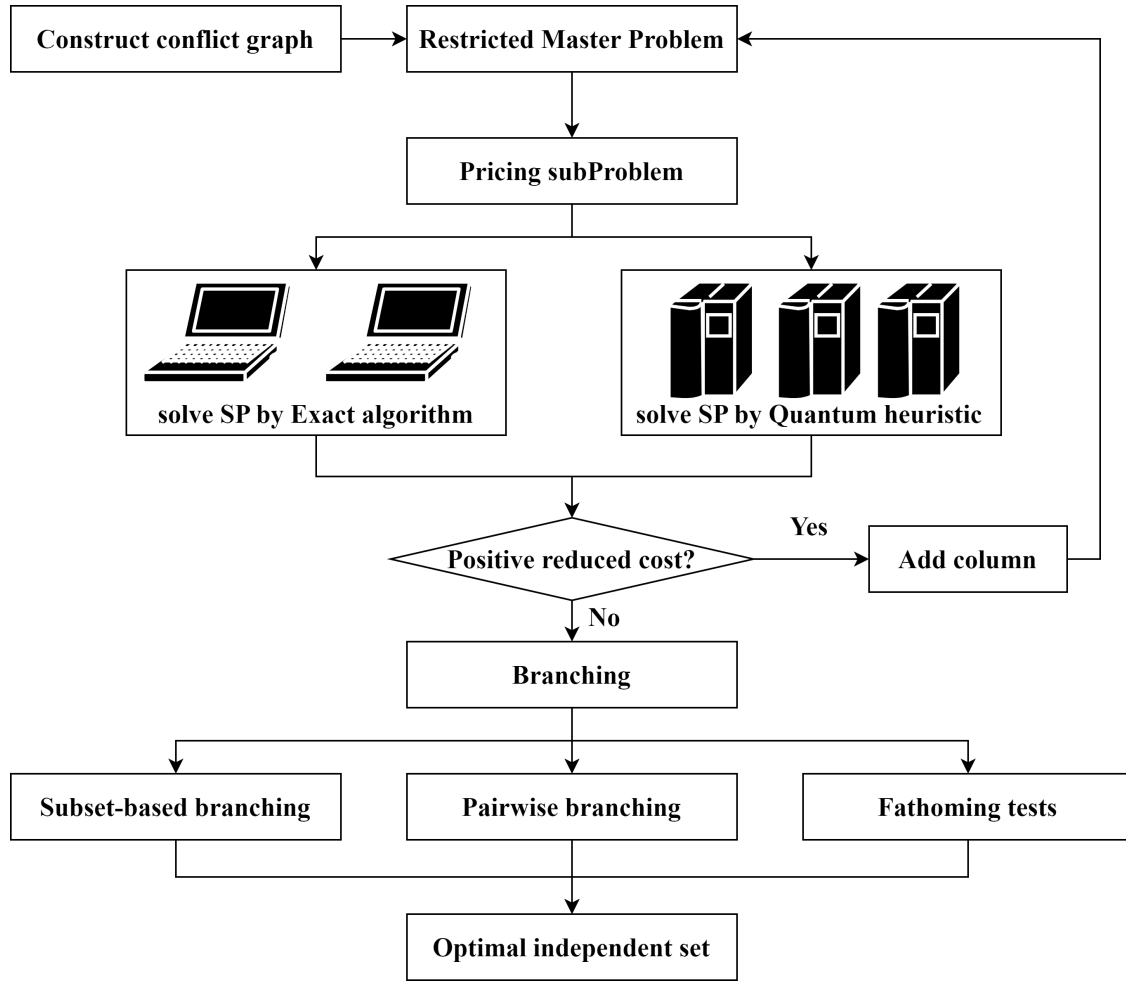


Figure 4: Overview of the proposed solution framework for the EV charging scheduling problem.

4.1 ILP Formulations

Restricted Master Problem

The RMP selects candidate independent sets within a Branch-and-Price framework by solving a linear relaxation. Let \mathcal{S}' denote the current set of generated independent sets, $\mathcal{C} = \{1, \dots, C\}$ the available charging piles, V the vertices of the conflict graph, and $P_n \subseteq V$ the partition corresponding to vehicle $n \in N$. The decision variable $\zeta_{S,c}$ indicates the extent to which the independent set S is selected and assigned to pile c , while τ represents the global latest charging completion time.

$$\min_{\tau, \zeta} \tau \quad (1)$$

subject to

$$\sum_{S \in \mathcal{S}'} \sum_{v \in S} \sum_{c \in \mathcal{C}} e_v \zeta_{S,c} \leq \tau, \quad \forall v \in V, \quad (2)$$

$$\sum_{S \in \mathcal{S}'} \sum_{c \in \mathcal{C}} \zeta_{S,c} = 1, \quad \forall n \in N, \quad (3)$$

$$\sum_{S \in \mathcal{S}'} \zeta_{S,c} \leq 1, \quad \forall (u, v) \in \mathcal{E}^A, \forall c \in \mathcal{C}, \quad (4)$$

$$\zeta_{S,c} \geq 0, \quad \forall S \in \mathcal{S}', \forall c \in \mathcal{C}, \quad (5)$$

$$\tau \geq 0. \quad (6)$$

Constraint (2) ensures that the completion time of each selected interval does not exceed τ . Constraint (3) enforces one selected interval per vehicle. Constraint (4) prevents conflicting intervals from being assigned to the same pile. Constraints (5)–(6) define variable domains.

Pricing Subproblem

Given an optimal dual solution (π, λ) of the relaxed RMP, where π_v and λ_n are associated with constraints (2) and (3), the reduced cost of a candidate column $S \subseteq V$ is

$$\text{rc}(S) = \sum_{v \in S} \pi_v e_v - \sum_{n \in N: S \cap P_n \neq \emptyset} \lambda_n. \quad (7)$$

For each vertex $v \in \mathcal{V}$, define its vertex-level contribution to the reduced cost as

$$\omega_v := \pi_v e_v - \lambda_{p(v)}. \quad (8)$$

Let $\mathcal{C} = \{1, \dots, C\}$ denote the set of charging piles, \mathcal{E}^A the set of conflict edges, and \mathcal{P} the set of vehicles. Introduce the binary decision variables

$$x_{v,c} = \begin{cases} 1, & \text{if vertex } v \text{ is assigned to pile } c, \\ 0, & \text{otherwise,} \end{cases} \quad (9)$$

$$y_c = \begin{cases} 1, & \text{if pile } c \text{ is used,} \\ 0, & \text{otherwise.} \end{cases} \quad (10)$$

The pricing subproblem is then formulated as

$$\max_{x, y} \sum_{v \in \mathcal{V}} \sum_{c \in \mathcal{C}} \omega_v x_{v,c} - \alpha \sum_{c \in \mathcal{C}} y_c \quad (11)$$

subject to

$$\sum_{v \in \mathcal{V}_p} \sum_{c \in \mathcal{C}} x_{v,c} = 1, \quad \forall p \in \mathcal{P}, \quad (12)$$

$$x_{u,c} + x_{v,c} \leq y_c, \quad \forall (u, v) \in \mathcal{E}^A, \forall c \in \mathcal{C}, \quad (13)$$

$$x_{v,c} \leq y_c, \quad \forall v \in \mathcal{V}, \forall c \in \mathcal{C}, \quad (14)$$

$$\sum_{c \in \mathcal{C}} y_c \leq C, \quad (15)$$

$$x_{v,c} \in \{0, 1\}, \quad \forall v \in \mathcal{V}, \forall c \in \mathcal{C} \quad (16)$$

$$y_c \in \{0, 1\}, \quad \forall c \in \mathcal{C} \quad (17)$$

Any optimal solution (x^*, y^*) induces an independent set

$$S = \{v \in \mathcal{V} \mid \exists c, x_{v,c}^* = 1\}, \quad (18)$$

with reduced cost $rc(S) < 0$, which is then added to the RMP. The y_c variables are auxiliary, ensuring pile feasibility but not affecting the reduced cost computation.

4.2 QUBO Formulation for the Pricing Subproblem

The pricing subproblem can be further transformed into a QUBO model, which can be solved using the QAIA implemented in the MindQuantum framework.

The objective of the pricing subproblem is to maximize the total weight of selected vertices, which can be expressed in QUBO form as

$$\mathcal{H}_0 = - \sum_{v \in \mathcal{V}} \sum_{c \in \mathcal{C}} \omega_v x_{v,c}, \quad (19)$$

where ω_v is the vertex-level contribution defined in the pricing subproblem.

The constraints of the original pricing problem are incorporated as quadratic penalties. The partition constraint, requiring exactly one vertex per vehicle, is represented by

$$\mathcal{H}_1 = \sum_{p \in \mathcal{P}} \lambda_1 \left(\sum_{v \in \mathcal{V}_p} \sum_{c \in \mathcal{C}} x_{v,c} - 1 \right)^2, \quad (20)$$

where λ_1 is a sufficiently large penalty coefficient.

The conflict constraint, preventing two adjacent or overlapping vertices from being assigned to the same charger, is enforced by

$$\mathcal{H}_2 = \sum_{c \in \mathcal{C}} \sum_{(u,v) \in \mathcal{E}^A} \lambda_2 x_{u,c} x_{v,c}, \quad (21)$$

with λ_2 chosen large enough to prevent conflicts.

The total QUBO Hamiltonian is then

$$\mathcal{H} = \mathcal{H}_0 + \mathcal{H}_1 + \mathcal{H}_2. \quad (22)$$

Solving (22) yields a binary assignment $\hat{x}_{v,c} \in \{0, 1\}$. A feasible independent set

$$S = \{v \in \mathcal{V} \mid \hat{x}_{v,c} = 1 \text{ for some } c\}$$

is obtained by first aggregating the selected vertices over chargers and then applying a greedy repair procedure in which, for any pair of conflicting vertices in \mathcal{E}^A , only the vertex with larger weight ω_v is retained, and the one-vertex-per-vehicle constraint is enforced by keeping the maximum-weight vertex in each partition P_n . This repaired independent set constitutes a new column added to the RMP in the column generation procedure.

In the QUBO formulation, the auxiliary variables y_c are omitted, as charger assignment feasibility is ensured by the greedy repair procedure applied after obtaining the binary solution $\hat{x}_{v,c}$.

4.3 Branching Scheme

To systematically explore the solution space in the Branch-and-Price framework for the EV charging scheduling problem, we design a complete branching scheme that respects both the conflict graph structure and the partition constraints corresponding to vehicles. The scheme consists of two sequential branching rules: a subset-based branching and a pairwise branching [40].

Subset-based Branching

Let P_n denote the set of candidate intervals for vehicle $n \in N$. At any branching node, if a partition P_n contains multiple fractionally selected vertices

$$\left| \left\{ v \in P_n : \sum_{S \in \mathcal{S}', v \in S} \zeta_S^* > 0 \right\} \right| > 1, \quad (23)$$

We select the vehicle n^* with the largest number of fractional vertices. Within P_{n^*} , the vertex

$$v^* = \arg \max_{v \in P_{n^*}} \sum_{S \in \mathcal{S}', v \in S} \zeta_S^* \quad (24)$$

is chosen for branching.

Two complementary child nodes are generated:

- **Select-branch:** vertex v^* is fixed as the chosen interval for vehicle n^* , and all other vertices in $P_{n^*} \setminus \{v^*\}$ are excluded from consideration.
- **Discard-branch:** vertex v^* is forbidden and removed from further consideration.

This rule ensures that each vehicle eventually has exactly one selected interval, and it does not alter the structure of the pricing problem.

Pairwise Branching

After applying the first rule, some partitions may still produce a fractional RMP solution. In this case, there exists at least one pair of vertices (u, v) from different partitions such that

$$0 < \sum_{S \in \mathcal{S}', u, v \in S} \zeta_S^* < 1, \quad (25)$$

called a *fractionally co-occurring pair*. We select the pair (u^*, v^*) with the largest fractional contribution for branching.

Two child nodes are created:

- **Different-color branch:** enforce that u^* and v^* cannot be selected simultaneously. This is implemented by adding an edge (u^*, v^*) to the conflict graph.
- **Same-color branch:** enforce that u^* and v^* must be selected together. A new super-vertex z is created to replace u^* and v^* , with edges

$$(z, w) \in E \quad \text{if } (u^*, w) \in E \text{ or } (v^*, w) \in E. \quad (26)$$

The partitions of u^* and v^* are merged, effectively binding the two vehicles to a common interval selection structure.

Fathoming Criteria and Completeness

A branch is pruned if the current solution becomes infeasible or the lower bound of the partial solution exceeds the global best known upper bound. By sequentially applying the two branching rules, each vehicle ultimately has exactly one selected interval, while all fractional RMP solutions are eliminated. Throughout the search process, the structure of the pricing subproblem is preserved, ensuring both the completeness of the branching scheme and the consistency of the solution procedure.

5 Computational results

5.1 Instances

All experiments were conducted on a Windows 10 PC with a 12th-generation Intel[®] Core[™] i7-12700H processor, using Python 3.10.18 (64-bit). A set of benchmark instances for the PCP was generated based on the EV charging scheduling scenario. Let T denote the scheduling horizon, d the fixed charging duration, N the number of vehicles, and C the number of charging piles. For each vehicle $i \in \{1, \dots, N\}$, K candidate charging start times $s_{i,k}$ were sampled uniformly at random from $[0, T - d]$, yielding intervals $[s_{i,k}, s_{i,k} + d]$. By fixing $|V|$ (the total number of intervals) and K , the number of vehicles is $N = |V|/K$. Each interval corresponds to a vertex in the PCP graph, and

vertices of the same vehicle form a partition. Conflict edges connect vertices either within the same partition or between overlapping intervals of different vehicles, respecting the charging pile capacity C .

All instances used $T = 24$, $d = 3$, and $C \in \{5, 10\}$. They were stored in text format with metadata recording time windows and partition indices. Files follow the naming convention $vVcCKsS$, where V is the number of vehicles, C the number of piles, K the number of candidate intervals per vehicle, and S the random seed. The maximum computational time per instance was 3600 seconds; if this limit was reached, the solver returned the incumbent best feasible solution.

5.2 Numerical results

In this subsection, we numerically evaluate the proposed branch-and-price framework on the EV charging PCP instances described in Section 5.1. We compare three variants of the algorithm:

1. **Gurobi (baseline)**: both the RMP and the pricing subproblem are formulated and solved by the classical MIP solver Gurobi.
2. **BSB**: the RMP is still solved by Gurobi, while the pricing subproblem is solved by the ballistic simulated branching algorithm `mindquantum.algorithm.qaia.BSB`.
3. **SimCIM**: the RMP is solved by Gurobi and the pricing subproblem is solved by the simulated coherent Ising machine algorithm `mindquantum.algorithm.qaia.SimCIM`.

For brevity, we refer to the two QAIA-based variants simply as BSB and SimCIM in what follows.

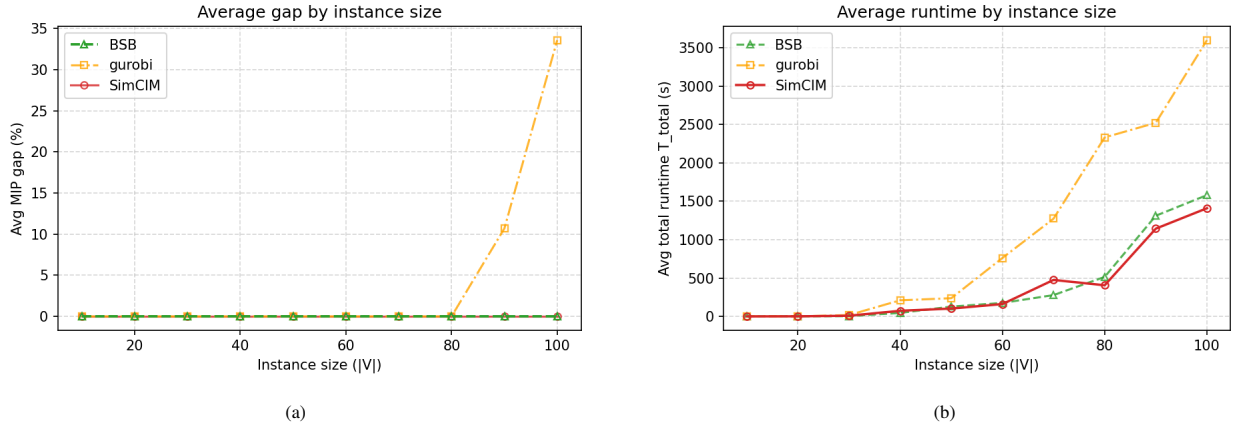


Figure 5: Scalability comparison of branch-and-price variants. (a) MIP gap versus instance size, showing that QAIA-based methods (BSB and SimCIM) consistently achieve zero optimality gap across all instances, while the Gurobi baseline exhibits rapidly increasing gaps for large-scale cases. (b) Total runtime versus instance size, where all methods perform similarly on small instances, but BSB and SimCIM scale significantly better than the baseline as problem size increases.

For each instance and each method, Tables 1–3 report the following performance indicators. Columns $|\mathcal{V}|$, $|\mathcal{E}|$, and N denote the number of vertices, edges, and vehicles (partitions), respectively. Column $Obj.$ gives the best objective value at termination, and Gap (%) is the relative optimality gap reported by the solver; a value of zero indicates that global optimality has been proved. The column T_{total} reports the wall-clock time (in seconds) spent inside the branch-and-price procedure, from the construction of the initial RMP until the last node is processed; it includes all calls to the MIP solver and the control logic of column generation, but excludes instance reading and final printing.

We further decompose the solver time into two components: T_{RMP} is the cumulative time spent solving all restricted master problems, and $T_{pricing}$ is the cumulative time spent solving all pricing subproblems. Finally, N_p denotes the number of pricing calls, N_c the number of generated columns, and N_n the number of processed branch-and-price nodes. Tables 1, 2, and 3 report these quantities for the Gurobi baseline, BSB, and SimCIM, respectively.

On *small and medium* instances ($V \leq 40$), all three methods can find and prove the global optimum, i.e., $gap = 0$ for all instances. The total runtime T_{total} is in the sub-second to tens-of-seconds range for all methods. In this regime, replacing the classical Gurobi pricing with BSB or SimCIM does not deteriorate solution quality and leads to comparable running times. Small variations in T_{total} mainly stem from differences in the number of pricing calls and the efficiency of the respective pricing solvers, but overall, all three methods behave similarly on these easier instances.

Table 1: Computational results of the instances solved by Gurobi

Instance	$ \mathcal{V} $	$ \mathcal{E} $	N	Obj.	Gap (%)	T_{total}	T_{RMP}	T_{pricing}	N_p	N_c	N_n
v10c5k2s1	10	11	5	18	0.00	0.59	0.04	0.52	39	1 224	10
v10c5k2s2	10	15	5	21	0.00	0.49	0.04	0.43	34	2 310	8
v10c5k2s3	10	22	5	21	0.00	0.76	0.06	0.67	63	3 868	17
v20c5k2s1	20	39	10	18	0.00	0.71	0.23	0.41	36	4 587	12
v20c5k2s2	20	46	10	21	0.00	0.69	0.19	0.46	29	8 263	9
v20c5k2s3	20	57	10	21	0.00	0.75	0.16	0.53	24	11 321	8
v30c5k3s1	30	118	10	17	0.00	11.89	3.30	7.80	252	50 607	77
v30c5k3s2	30	108	10	17	0.00	29.02	8.91	17.41	1 295	201 841	461
v30c5k3s3	30	123	10	18	0.00	11.92	3.77	7.15	325	262 858	104
v40c5k4s1	40	205	10	15	0.00	346.50	139.39	167.50	3 229	597 481	1 055
v40c5k4s2	40	219	10	15	0.00	169.20	64.38	88.38	1 626	922 675	495
v40c5k4s3	40	197	10	15	0.00	114.99	53.62	47.47	1 037	1 146 298	321
v50c10k5s1	50	320	10	10	0.00	136.28	53.89	74.26	744	305 519	230
v50c10k5s2	50	342	10	14	0.00	366.65	153.63	183.80	4 158	1 354 840	1 306
v50c10k5s3	50	338	10	12	0.00	208.38	80.11	116.46	1 295	1 819 533	382
v60c10k6s1	60	490	10	10	0.00	259.33	105.56	138.27	1 444	486 050	467
v60c10k6s2	60	509	10	14	0.00	1 047.50	461.93	505.34	10 084	3 060 585	3 305
v60c10k6s3	60	512	10	10	0.00	976.85	377.42	546.14	2 953	1 156 494	856
v70c10k7s1	70	696	10	10	0.00	2 674.72	1 248.74	1 236.48	17 403	5 463 412	5 557
v70c10k7s2	70	710	10	10	0.00	406.67	183.62	203.44	1 358	6 095 377	396
v70c10k7s3	70	679	10	12	0.00	740.31	352.93	352.04	2 021	7 337 643	542
v80c10k8s1	80	918	10	6	0.00	2 367.23	1 318.34	731.75	2 829	1 875 064	861
v80c10k8s2	80	904	10	11	0.00	1 472.33	768.11	598.06	6 492	4 304 470	2 161
v80c10k8s3	80	891	10	12	0.00	3 158.11	1 572.39	1 410.68	9 101	9 114 941	2 719
v90c10k9s1	90	1 164	10	10	32.08	3 600.02	1 827.34	1 623.28	5 513	4 062 436	1 664
v90c10k9s2	90	1 137	10	11	0.00	820.15	312.43	490.66	249	4 509 936	62
v90c10k9s3	90	1 144	10	6	0.00	3 149.07	1 603.51	1 407.98	4 801	3 477 710	1 350
v100c10k10s1	100	1 437	10	14	35.71	3 600.47	1 870.14	1 563.06	4 849	3 619 512	1 469
v100c10k10s2	100	1 372	10	12	25.00	3 600.07	2 209.08	1 220.32	4 185	7 291 623	1 280
v100c10k10s3	100	1 398	10	15	40.00	3 600.31	1 551.81	1 955.20	368	8 098 615	97

The benefit of QAIA-based pricing becomes pronounced on *large and hard* instances ($V \geq 80$). For several of the largest instances, the pure Gurobi baseline hits the time limit of 3600 s and terminates with a non-zero optimality gap (up to about 35–40% on some $V = 100$ instances), as shown in Table 1. In contrast, both BSB and SimCIM are able to close the gap and prove optimality within the same time limit, often with a significantly smaller total runtime. For example, for instance v100c10k10s1, the baseline method stops at $T_{\text{total}} \approx 3600$ s with a large remaining gap, whereas BSB and SimCIM reach the optimal solution with gap = 0 in roughly 900–1000 s. Similar patterns can be observed in other $V = 80, 90, 100$ instances: the two QAIA-based methods consistently match the best objective values of the baseline and, in many of the hardest cases, convert “time-limit with gap” runs of Gurobi into fully optimal solutions.

The overall trends are further illustrated in Figures 5 (a) and Figures 5 (b), which plot the MIP gap and total runtime as a function of the instance size $|V|$ for the three methods. Figures 5 (a) shows that BSB and SimCIM achieve gap = 0 on all tested instances, while the Gurobi baseline exhibits large positive gaps only on the largest instances. Figures 5 (b) indicates that all methods have similar runtimes on small instances, but as $|V|$ grows, the total runtime of the baseline method increases much faster than that of the QAIA-based methods. In particular, for the largest instances, the BSB and SimCIM curves stay well below the 3600 s time limit, whereas the baseline curve often saturates at the time limit.

These observations suggest that QAIA-based pricing improves the effectiveness of the column generation and branching process. Although the detailed internal statistics are not all shown in the figures, Tables 1–3 and the logs indicate that BSB and SimCIM typically generate a large number of high-quality columns within a moderate number of pricing calls, enabling the RMP to capture the structure of the problem more quickly and allowing the branch-and-price tree to be explored with fewer or comparable processed nodes while still certifying optimality. Comparing the two QAIA variants, BSB generally achieves slightly smaller or comparable T_{total} on many of the larger instances, while SimCIM provides

Table 2: Computational results of instances solved by the BSB method

Instance	$ \mathcal{V} $	$ \mathcal{E} $	N	Obj.	Gap (%)	T_{total}	T_{RMP}	T_{pricing}	N_p	N_c	N_n
v10c5k2s1	10	11	5	18	0.00	0.13	0.03	0.08	35	891	8
v10c5k2s2	10	15	5	21	0.00	0.12	0.03	0.08	34	1 608	10
v10c5k2s3	10	22	5	21	0.00	0.11	0.03	0.07	33	2 211	8
v20c5k2s1	20	39	10	18	0.00	2.07	1.04	0.80	60	6 154	18
v20c5k2s2	20	46	10	21	0.00	0.54	0.28	0.18	34	9 808	12
v20c5k2s3	20	57	10	21	0.00	0.32	0.17	0.11	29	13 123	10
v30c5k3s1	30	118	10	17	0.00	3.47	2.26	0.75	197	31 870	72
v30c5k3s2	30	108	10	17	0.00	4.07	2.55	0.98	266	69 548	105
v30c5k3s3	30	123	10	18	0.00	2.25	1.52	0.46	98	90 877	37
v40c5k4s1	40	205	10	15	0.00	10.34	7.52	1.55	79	33 518	30
v40c5k4s2	40	219	10	15	0.00	24.34	16.66	4.15	215	96 163	82
v40c5k4s3	40	197	10	15	0.00	102.66	62.39	25.15	1 895	402 235	728
v50c10k5s1	50	320	10	10	0.00	54.79	40.01	9.25	909	233 195	337
v50c10k5s2	50	342	10	14	0.00	161.77	116.58	27.57	2 401	814 713	934
v50c10k5s3	50	338	10	12	0.00	166.67	126.93	21.10	393	999 817	151
v60c10k6s1	60	490	10	10	0.00	97.52	72.02	15.44	1 870	320 294	759
v60c10k6s2	60	509	10	14	0.00	334.88	249.28	50.21	4 704	1 605 097	1 868
v60c10k6s3	60	512	10	10	0.00	95.43	77.96	9.14	447	1 834 619	177
v70c10k7s1	70	696	10	10	0.00	428.59	336.82	53.66	4 467	1 163 328	1 758
v70c10k7s2	70	710	10	10	0.00	159.92	136.59	12.06	499	1 478 417	184
v70c10k7s3	70	679	10	12	0.00	245.35	211.69	18.39	687	1 962 177	273
v80c10k8s1	80	918	10	6	0.00	283.31	250.68	16.46	518	438 516	195
v80c10k8s2	80	904	10	11	0.00	406.65	342.71	34.52	1 860	1 298 232	743
v80c10k8s3	80	891	10	12	0.00	854.50	727.35	69.19	2 754	3 004 040	1 072
v90c10k9s1	90	1 164	10	7	0.00	1 241.05	1 115.71	66.23	1 748	1 573 060	688
v90c10k9s2	90	1 137	10	11	0.00	853.65	762.13	42.38	997	2 623 423	392
v90c10k9s3	90	1 144	10	6	0.00	1 842.04	1 588.64	130.23	4 625	2 969 128	1 736
v100c10k10s1	100	1 437	10	10	0.00	965.76	844.34	62.93	4 616	1 304 499	1 844
v100c10k10s2	100	1 372	10	10	0.00	3 217.70	2 707.04	282.36	17 780	7 342 087	7 027
v100c10k10s3	100	1 398	10	10	0.00	558.98	517.09	18.68	383	7 832 319	152

similar solution quality and often comparable performance, acting as a complementary quantum-inspired heuristic. Overall, embedding MindQuantum’s QAIA solvers (realized here as BSB and SimCIM) into the pricing subproblem of a classical branch-and-price framework yields a robust hybrid algorithm: on small and medium instances, it matches the performance of the pure Gurobi baseline, and on large and difficult instances, it significantly improves scalability and robustness by delivering high-quality (often provably optimal) solutions within much shorter runtimes than the classical baseline.

6 Conclusions

In this manuscript, we studied an intra-day electric vehicle charging scheduling problem and formulated it as a Partition Coloring Problem. Vehicles are modeled as partitions, candidate charging intervals as vertices, and temporal or resource conflicts as edges in a conflict graph. This representation makes the one-interval-per-vehicle requirement and charger capacity constraints explicit and is well-suited to instances with many alternative intervals.

Building on this formulation, we propose a hybrid quantum–classical branch-and-price algorithm. The restricted master problem is solved by Gurobi, while the pricing subproblem is cast as a maximum independent set problem and further reformulated as a QUBO model to be tackled by QAIA. Two QAIA-based pricing schemes, using BSB and SimCIM, were implemented within the MindQuantum framework and compared with a pure Gurobi-based branch-and-price baseline.

Numerical experiments on synthetic benchmark instances show that all three methods obtain optimal solutions with comparable runtimes on small and medium problems. For large and difficult instances, however, the QAIA-enhanced

Table 3: Computational results of instances solved by the SimCIM method

Instance	$ \mathcal{V} $	$ \mathcal{E} $	N	Obj.	Gap (%)	T_{total}	T_{RMP}	T_{pricing}	N_p	N_c	N_n
v10c5k2s1	10	11	5	18	0.00	0.14	0.04	0.09	36	950	7
v10c5k2s2	10	15	5	21	0.00	0.18	0.05	0.13	52	2 011	10
v10c5k2s3	10	22	5	21	0.00	0.15	0.04	0.10	40	2 765	8
v20c5k2s1	20	39	10	18	0.00	0.95	0.46	0.42	111	11 406	23
v20c5k2s2	20	46	10	21	0.00	1.60	0.73	0.72	182	27 629	47
v20c5k2s3	20	57	10	21	0.00	0.80	0.38	0.37	85	36 912	13
v30c5k3s1	30	118	10	17	0.00	9.42	5.03	3.84	672	140 893	60
v30c5k3s2	30	108	10	17	0.00	4.20	2.26	1.70	280	203 937	29
v30c5k3s3	30	123	10	18	0.00	13.81	7.18	6.06	1 001	419 810	61
v40c5k4s1	40	205	10	15	0.00	69.15	38.26	26.92	4 859	1 054 133	567
v40c5k4s2	40	219	10	15	0.00	69.41	39.12	26.03	4 518	2 085 768	497
v40c5k4s3	40	197	10	15	0.00	81.63	44.23	32.15	6 121	3 309 729	887
v50c10k5s1	50	320	10	10	0.00	39.62	27.81	8.22	503	179 936	125
v50c10k5s2	50	342	10	14	0.00	183.99	121.77	47.44	2 998	1 140 887	621
v50c10k5s3	50	338	10	12	0.00	83.81	58.07	19.03	1 219	1 536 352	295
v60c10k6s1	60	490	10	10	0.00	68.95	47.99	14.81	1 596	241 241	505
v60c10k6s2	60	509	10	14	0.00	309.76	218.84	65.62	3 885	1 523 498	1 121
v60c10k6s3	60	512	10	10	0.00	104.12	82.42	13.21	596	1 796 870	200
v70c10k7s1	70	696	10	10	0.00	767.03	582.54	123.22	7 099	2 424 686	2 234
v70c10k7s2	70	710	10	10	0.00	411.35	328.28	52.47	2 400	3 466 319	797
v70c10k7s3	70	679	10	12	0.00	248.01	197.73	37.25	1 039	4 314 303	194
v80c10k8s1	80	918	10	6	0.00	441.98	374.12	39.50	1 794	787 934	682
v80c10k8s2	80	904	10	11	0.00	444.22	363.58	49.50	2 569	1 822 835	883
v80c10k8s3	80	891	10	12	0.00	331.01	287.02	26.55	698	2 454 506	209
v90c10k9s1	90	1 164	10	7	0.00	742.89	650.83	50.88	1 387	1 093 815	493
v90c10k9s2	90	1 137	10	11	0.00	853.12	756.72	47.85	1 002	2 149 515	392
v90c10k9s3	90	1 144	10	6	0.00	1 834.94	1 567.18	147.81	4 646	5 130 084	1 711
v100c10k10s1	100	1 437	10	10	0.00	968.25	835.83	74.32	5 049	1 344 067	1 893
v100c10k10s2	100	1 372	10	10	0.00	2 726.95	2 380.15	183.05	4 633	5 508 556	1 759
v100c10k10s3	100	1 398	10	10	0.00	534.31	491.69	20.21	383	5 998 788	152

variants achieve markedly better scalability: they often close optimality gaps and prove optimality within the time limit in cases where the baseline hits the limit with sizable gaps. Overall, the results suggest that embedding QAIA in classical decomposition algorithms is an effective way to improve the practical solvability of large-scale EV charging scheduling and related PCP models. Future work will consider richer network constraints, data-driven instance generation, and the integration of other quantum-inspired or variational algorithms within the same framework.

References

- [1] Alexandre Dolgui, Sergey Kovalev, and Mikhail Y Kovalyov. Scheduling electric vehicle regular charging tasks: A review of deterministic models. *European Journal of Operational Research*, 325(2):221–232, 2025.
- [2] Senlei Wang, Janody Pougala, and Tim Hillel. Joint modelling of electric vehicle charging and daily activity scheduling. *Available at SSRN 5143388*, 2024.
- [3] Shiwei Shen, Syed Irtaza Haider, Razan Habeeb, and Frank HP Fitzek. Coordinating day-ahead and intraday scheduling for bidirectional charging of fleet evs. *Automation*, 6(4):64, 2025.
- [4] Raviteja Chemudupaty, Timothée Hornek, Ivan Pavić, and Sergio Potenciano Menci. Optimizing trading of electric vehicle charging flexibility in the continuous intraday market under user and market uncertainties. *Applied Energy*, 381:125103, 2025.
- [5] Penghui Xu, Xiaobo Wang, and Zhichao Li. Impact and optimization of vehicle charging scheduling on regional clean energy power supply network management. *Energy Informatics*, 8(1):13, 2025.

- [6] Christos D Korkas, Christos D Tsaknakis, Athanasios Ch Kapoutsis, and Elias Kosmatopoulos. Distributed and multi-agent reinforcement learning framework for optimal electric vehicle charging scheduling. *Energies (19961073)*, (15), 2024.
- [7] Ji Wu, Hao Su, Jinhao Meng, and Mingqiang Lin. Electric vehicle charging scheduling considering infrastructure constraints. *Energy*, 278:127806, 2023.
- [8] Rodolphe Griset and Joseph Mikael. Software suite for benchmarking of quantum algorithms applied to two typical smart-charging optimization problems. 2024.
- [9] Fabio Furini, Enrico Malaguti, and Alberto Santini. An exact algorithm for the partition coloring problem. *Computers & Operations Research*, 92:170–181, 2018.
- [10] Enqiang Zhu, Fei Jiang, Chanjuan Liu, and Jin Xu. Partition independent set and reduction-based approach for partition coloring problem. *IEEE Transactions on Cybernetics*, 52(6):4960–4969, 2020.
- [11] Oylum Şeker, Neda Tanoumand, and Merve Bodur. Digital annealer for quadratic unconstrained binary optimization: a comparative performance analysis. *Applied Soft Computing*, 127:109367, 2022.
- [12] Vincent F Yu, Pham Tuan Anh, and Yu-Wei Chen. The electric vehicle routing problem with time windows, partial recharges, and parcel lockers. *Applied Sciences*, 13(16):9190, 2023.
- [13] Ugur Bac and Mehmet Erdem. Optimization of electric vehicle recharge schedule and routing problem with time windows and partial recharge: A comparative study for an urban logistics fleet. *Sustainable Cities and Society*, 70:102883, 2021.
- [14] Cristian Cataldo-Díaz, Rodrigo Linfati, and John Willmer Escobar. Mathematical models for the electric vehicle routing problem with time windows considering different aspects of the charging process. *Operational Research*, 24(1):1, 2024.
- [15] YINGKAI XU. Electric vehicle routing problem: A review of recent approaches and algorithms. *Studia Universitatis Babeş-Bolyai, Informatica*, 69(2), 2024.
- [16] Aiping Tan, Chang Wang, Yan Wang, and Chenglong Dong. Electric vehicle charging route planning for shortest travel time based on improved ant colony optimization. *Sensors*, 25(1):176, 2024.
- [17] Nima Moradi, Niloufar Mirzavand Boroujeni, Navid Aftabi, and Amin Aslani. Two-echelon electric vehicle routing problem in parcel delivery: A literature review. *arXiv preprint arXiv:2412.19395*, 2024.
- [18] Mohsen Dastpak, Fausto Errico, Ola Jabali, and Federico Malucelli. Dynamic routing for the electric vehicle shortest path problem with charging station occupancy information. *Transportation Research Part C: Emerging Technologies*, 158:104411, 2024.
- [19] Haoyu Li, Jihuang Chen, Chao Yang, Xin Chen, Le Chang, and Jiabei Liu. Smart and efficient ev charging navigation scheme in vehicular edge computing networks. *Journal of Cloud Computing*, 12(1):176, 2023.
- [20] Axel Parmentier, Rafael Martinelli, and Thibaut Vidal. Electric vehicle fleets: Scalable route and recharge scheduling through column generation. *Transportation Science*, 57(3):631–646, 2023.
- [21] Yongsun Zang, Meiqin Wang, and Mingyao Qi. A column generation tailored to electric vehicle routing problem with nonlinear battery depreciation. *Computers & Operations Research*, 137:105527, 2022.
- [22] Yannick Deller, Sebastian Schmitt, Maciej Lewenstein, Steve Lenk, Marika Federer, Fred Jendrzejewski, Philipp Hauke, and Valentin Kasper. Quantum approximate optimization algorithm for qudit systems. *Physical Review A*, 107(6):062410, 2023.
- [23] Zhonghao Zhao, Carman KM Lee, Xiaoyuan Yan, and Haonan Wang. Reinforcement learning for electric vehicle charging scheduling: A systematic review. *Transportation Research Part E: Logistics and Transportation Review*, 190:103698, 2024.
- [24] Guangzhi Li and Rahul Simha. The partition coloring problem and its application to wavelength routing and assignment. In *Proceedings of the First Workshop on Optical Networks*, volume 1. Dallas, 2000.
- [25] Oylum Şeker, Tınaz Ekim, and Z Caner Taşkın. A decomposition approach to solve the selective graph coloring problem in some perfect graph families. *Networks*, 73(2):145–169, 2019.
- [26] Oylum Şeker, Tınaz Ekim, and Z. Caner Taşkın. An exact cutting plane algorithm to solve the selective graph coloring problem in perfect graphs. *European Journal of Operational Research*, 291(1):67–83, 2021.
- [27] Emanuel Florentin Olariu and Cristian Frăsinaru. A set packing model for the partition coloring problem. *Carpathian Journal of Mathematics*, 41(2):465–477, 2025.
- [28] Stefka Fidanova and Petrică C Pop. An ant algorithm for the partition graph coloring problem. In *International Conference on Numerical Methods and Applications*, pages 78–84. Springer, 2014.

- [29] Ahmed Kheiri, Rhyd Lewis, Jonathan Thompson, and Paul Harper. Constructing operating theatre schedules using partitioned graph colouring techniques. *Health Systems*, 10(4):286–297, 2021.
- [30] Andrew Lucas. Ising formulations of many np problems. *Frontiers in physics*, 2:5, 2014.
- [31] Peter L McMahon, Alireza Marandi, Yoshitaka Haribara, Ryan Hamerly, Carsten Langrock, Shuhei Tamate, Takahiro Inagaki, Hiroki Takesue, Shoko Utsunomiya, Kazuyuki Aihara, et al. A fully programmable 100-spin coherent ising machine with all-to-all connections. *Science*, 354(6312):614–617, 2016.
- [32] Maliheh Aramon, Gili Rosenberg, Elisabetta Valiante, Toshiyuki Miyazawa, Hirotaka Tamura, and Helmut G Katzgraber. Physics-inspired optimization for quadratic unconstrained problems using a digital annealer. *Frontiers in Physics*, 7:48, 2019.
- [33] Fuxi Cai, Suhas Kumar, Thomas Van Vaerenbergh, Xia Sheng, Rui Liu, Can Li, Zhan Liu, Martin Foltin, Shimeng Yu, Qiangfei Xia, et al. Power-efficient combinatorial optimization using intrinsic noise in memristor hopfield neural networks. *Nature Electronics*, 3(7):409–418, 2020.
- [34] William A Borders, Ahmed Z Pervaiz, Shunsuke Fukami, Kerem Y Camsari, Hideo Ohno, and Supriyo Datta. Integer factorization using stochastic magnetic tunnel junctions. *Nature*, 573(7774):390–393, 2019.
- [35] Egor S Tiunov, Alexander E Ulanov, and AI Lvovsky. Annealing by simulating the coherent ising machine. *Optics express*, 27(7):10288–10295, 2019.
- [36] Taro Kanao and Hayato Goto. Simulated bifurcation for higher-order cost functions. *Applied Physics Express*, 16(1):014501, 2022.
- [37] Dixiong Yang and Jilei Zhou. Connections among several chaos feedback control approaches and chaotic vibration control of mechanical systems. *Communications in Nonlinear Science and Numerical Simulation*, 19(11):3954–3968, 2014.
- [38] Timothée Leleu, Farad Khoystatee, Timothée Levi, Ryan Hamerly, Takashi Kohno, and Kazuyuki Aihara. Scaling advantage of chaotic amplitude control for high-performance combinatorial optimization. *Communications Physics*, 4(1):266, 2021.
- [39] Sam Reifenstein, Timothee Leleu, Timothy McKenna, Marc Jankowski, Myoung-Gyun Suh, Edwin Ng, Farad Khoystatee, Zoltan Toroczkai, and Yoshihisa Yamamoto. Coherent sat solvers: a tutorial. *Advances in Optics and Photonics*, 15(2):385–441, 2023.
- [40] Aleksandr Aleksandrovich Zykov. *On some properties of linear complexes*. Number 79. American Mathematical Society, 1952.